Molecular Therapy
Nucleic Acids
Original Article

Targeting oncogenic *KRAS* in non-small cell lung cancer with EGFR aptamer-conjugated multifunctional RNA nanoparticles

Linlin Yang,[1] Zhefeng Li,[2] Daniel W. Binzel,[2] Peixuan Guo,[2] and Terence M. Williams[1]

[1]Department of Radiation Oncology, Beckman Research Institute, City of Hope National Medical Center, Duarte, CA 91010, USA; [2]Center for RNA Nanobiotechnology and Nanomedicine, College of Pharmacy, James Comprehensive Cancer Center, Dorothy M. Davis Heart and Lung Research Institute, The Ohio State University, Columbus, OH 43210, USA

***KRAS* mutations are one of the most common oncogenic driver mutations in human cancers, including non-small cell lung cancer (NSCLC), and have established roles in cancer pathogenesis and therapeutic resistance. The development of effective inhibitors of mutant *KRAS* represents a significant challenge. Three-way junction (3WJ)-based multi-functional RNA nanoparticles have the potential to serve as an effective *in vivo* siRNA delivery platform with the ability to enhance tumor targeting specificity and visualize biodistribution through an imaging moiety. Herein, we assembled novel $EGFR_{apt}$-3WJ-si$KRAS^{G12C}$ mutation targeted nanoparticles to target EGFR-expressing human NSCLC harboring a $KRAS^{G12C}$ mutation to silence $KRAS^{G12C}$ expression in a tumor cell-specific fashion. We found that $EGFR_{apt}$-3WJ-si$KRAS^{G12C}$ nanoparticles potently depleted cellular $KRAS^{G12C}$ expression, resulting in attenuation of downstream MAPK pathway signaling, cell proliferation, migration/invasion ability, and sensitized NSCLC cells to chemoradiotherapy. *In vivo*, these nanoparticles induced tumor growth inhibition in $KRAS^{G12C}$ NSCLC tumor xenografts. Together, this study suggests that the 3WJ pRNA-based platform has the potential to suppress mutant KRAS activity for the treatment of KRAS-driven human cancers, and warrants further development for clinical translation.**

INTRODUCTION

Kirsten rat sarcoma viral oncogene homolog (*KRAS*) is a member of the human Ras gene family, encoding a small GTPase membrane-bound protein. KRAS functions as a binary molecular switch, cycling between a GDP-bound inactive and GTP-bound active state. *KRAS* mutations are widespread in human cancers, especially in three of the most lethal cancers: lung cancer, colorectal cancer, and pancreatic cancer.[1] Missense mutations of *KRAS*, most commonly at codons 12 and 13, aberrantly attenuate GTPase activity, resulting in accumulation of GTP-bound activated KRAS. The constitutively activated KRAS oncoproteins initiate downstream cellular signal transduction cascades irrespective of input from extracellular signals including mitogen-activated protein kinase (MAPK) and phosphatidylinositol 3-kinase pathways, leading to uncontrolled cell proliferation and abnormal cell survival, which are hallmarks of cancer.[2–5] Lung cancer is the leading cause of cancer-related deaths worldwide, with non-small cell lung cancer (NSCLC) accounting for 84% of all lung cancer diagnoses.[6] *KRAS* mutations occur in 20%–25% of NSCLC (most commonly in adenocarcinoma subtype), with $KRAS^{G12C}$ mutation being the most frequent mutation variant, accounting for approximately 39% of all *KRAS* mutations in NSCLC.[7–10]

A large body of research has reported that the presence of *KRAS* mutations promotes tumor cell-autonomous-mediated resistance to cancer therapeutics. For instance, cetuximab and panitumumab (monoclonal antibodies to EGFR) and EGFR tyrosine kinase inhibitors, such as erlotinib and gefitinib, are ineffective in *KRAS* mutant colorectal cancer and NSCLC, respectively, restricting their use to *KRAS* wild-type colorectal cancer and EGFR-mutant NSCLC.[11–17] While erlotinib is approved in combination with gemcitabine for pancreatic adenocarcinoma treatment, the combination produces minimal benefit in outcomes (only 2 weeks improved survival), likely due to the presence of *KRAS* mutations in 90%–95% of tumors leading to constitutive signaling downstream of the point of inhibition at EGFR.[18] In radiotherapy, a preclinical study in 1988 first documented that hyperactivation of Ras isoforms (including *KRAS*) leads to tumor-intrinsic radioresistance.[19] Emerging clinical evidence supports that *KRAS* mutations are associated with radiation resistance in colorectal and lung cancer.[20–22] Our recent studies and those of others have detailed some of the molecular mechanisms involved in KRAS activation promoting radiation resistance in colorectal and lung cancer.[22,23]

Due to the high prevalence and importance of *KRAS* mutations in human cancer, pharmaceutical companies and academic laboratories have tried for decades to identify small-molecule inhibitors of KRAS mutation, but little progress had been achieved and many had labeled KRAS as "undruggable." However, beginning in 2013, Shokat and co-workers reported the identification of covalent small-molecule compounds to target the reactive cysteine-12 of $KRAS^{G12C}$.[24] Based on this finding,

Received 1 August 2022; accepted 25 July 2023;
https://doi.org/10.1016/j.omtn.2023.07.027.

Correspondence: Terence M. Williams, Department of Radiation Oncology, City of Hope National Medical Center, 1500 E. Duarte Road, Duarte, CA 91741, USA.
E-mail: terwilliams@coh.org

Janes et al. developed a covalent $KRAS^{G12C}$ inhibitor ARS-1620, which could induce NSCLC tumor regression in *in vivo* models.[25] Furthermore, Canon et al. expanded on the success of ARS-1620 to develop the compound named AMG 510,[26] which is the first molecule to enter the clinic (NCT03600883) and ultimately receive FDA approval for the treatment of $KRAS^{G12C}$ tumors. Recently, several other $KRAS^{G12C}$ covalent inhibitors are also in phase I/II clinical trials,[27] such as MRTX849, ARS-3248, and LY3499446 (NCT03785249, NCT04006301, and NCT04165031). As these covalent inhibitors require $KRAS^{G12C}$ to be in the GDP bound state, drug resistance could be induced by disabling the GTPase activity or promoting the guanine exchange of GDP for GTP.[27] Currently, small-molecular inhibitors that can target the plethora of other KRAS mutations (e.g., G12D, G12V, G12R, G13D, etc.) are either under-studied or in preclinical development.

The field of RNA nanotechnology has advanced rapidly during recent decades. It was first introduced in 1998, and the field encompasses the design, fabrication, and application of nanometer-scale RNA architectures.[28,29] RNA nanoparticles have the simplistic characteristic of DNA canonical base pairing, while containing the structural flexibility and functional diversity characteristics of proteins. Noncanonical base pairing, base stacking, and elaborate networks of tertiary contacts further expand RNA structure versatility while also increasing thermodynamic stability.[29] Yet the dynamic nature of RNA allows RNA nanoparticles to remain deformative and motile to lead to high tumor accumulation and rapid renal clearance for maximized therapeutic dose delivery and reduced toxicities.[30,31] Three-way junction (3WJ) packaging RNA (pRNA) is a novel type of RNA nanotechnology derived from the pRNA of the bacteriophage phi29 DNA packaging motor. 3WJ pRNA has been extensively studied to fabricate various RNA nanoparticles with precise control of shape, size, and stoichiometry. The extending arms of 3WJ pRNA structures could be intelligently replaced with small interfering RNAs (siRNAs), miRNAs, riboswitches, and RNA aptamers, and conjugated with fluorescent probes or other moieties to construct multi-functional pRNA nanoparticles.[32] Due to their great plasticity and stability, 3WJ pRNA nanoparticles are emerging as a highly desirable *in vivo* delivery system for targeted gene therapy in human cancers.[28,29,32]

In this study, we report the development of a multifunctional RNA nanoparticle, $EGFR_{apt}$-3WJ-Alexa647-si$KRAS^{G12C}$, to explore the potential of 3WJ pRNA nanoparticles to deliver siRNA targeting $KRAS^{G12C}$ into NSCLC cells. Overexpression of EGFR has been reported in many human cancers, including NSCLC.[33] Thus, we have engineered EGFR targeting RNA aptamers ($EGFR_{apt}$) to further enhance the tumor specificity of the technology. We find that our $EGFR_{apt}$-3WJ-si$KRAS^{G12C}$ nanoparticles exhibit high thermostability and demonstrate high efficiency to specifically silence $KRAS^{G12C}$ and suppress downstream signaling pathways. Importantly, these nanoparticles sensitized NSCLC cells to chemotherapy and radiation therapy, inhibited proliferation, migration, invasion, and suppressed tumor growth by systemic delivery in a heterotopic mouse model. This platform technology has the potential to be adapted to other RAS mutations, enabling high tumor specificity.

RESULTS

Construction and characterization of $EGFR_{apt}$-3WJ-si$KRAS^{G12C}$ nanoparticles

Utilizing the 3WJ of phi29 pRNA (3WJ pRNA) as the core scaffold, multifunctional $EGFR_{apt}$-3WJ-si$KRAS^{G12C}$ pRNA nanoparticles were constructed, harboring EGFR-targeting RNA aptamer, therapeutic $KRAS^{G12C}$ siRNA, and Alexa 647 as the imaging module (Figure 1A). When the four nanoparticle component strands were mixed in equal molar ratio in TMS buffer, the pRNA nanoparticles assembled with very high efficiency, as indicated by agarose gel shift assays, showing stepwise assembly of the pRNA nanoparticle (Figure 1B). Dynamic light scattering (DLS) analysis determined the diameter of the $EGFR_{apt}$-3WJ-si$KRAS^{G12C}$ RNA nanoparticles (RNPs) as 7.2 ± 0.5 nm (Figure 1C) compared with 4.2 ± 1.1 nm for the 3WJ pRNA core scaffold.[34] To assess thermodynamic parameters, the Alexa 647-labeled $EGFR_{apt}$-3WJ-si$KRAS^{G12C}$ RNPs were subjected to temperature gradient gel electrophoresis (TGGE). Alexa 647-labeled strands were used to determine the percentage of remaining intact nanoparticles as temperature gradient increased from 25°C to 80°C. We determined the melting temperature (T_m) of $EGFR_{apt}$-3WJ-si$KRAS^{G12C}$ nanoparticles as 51.77°C (Figure 1D), indicating that the constructed RNPs with all functional modules are thermostable.

$EGFR_{apt}$-3WJ-si$KRAS^{G12C}$ nanoparticles efficiently bind and deliver $KRAS^{G12C}$ siRNA to NSCLC cells

We next examined the EGFR-targeting capabilities of Alexa 647-conjugated $EGFR_{apt}$-3WJ-si$KRAS^{G12C}$ nanoparticles in $KRAS^{G12C}$ NSCLC cell lines H2030 and H2122. Flow cytometric analysis illustrated a significantly higher level of target cell association using the EGFRapt-3WJ-si$KRAS^{G12C}$ nanoparticles compared with 3WJ-si$KRAS^{G12C}$ nanoparticles and scrambled aptamer-conjugated pRNA nanoparticles (Figures 2A and S1A). To further confirm whether the observed improvement in pRNA nanoparticle uptake is dependent on EGFR aptamer, we evaluated the binding ability of pRNA nanoparticles to NSCLC after silencing EGFR expression by siRNA. We found that, compared with the non-targeting silencing control, the EGFR silencing induced by siRNA (confirmed in Figure S1B) reduced the binding ability of EGFRapt-3WJ-si$KRAS^{G12C}$ nanoparticles by 30% and 38% in H2030 and H2122 cell lines, respectively (Figures 2B and S1C). Interestingly, EGFR depletion also slightly reduced binding of SCRapt-3WJ-si$KRAS^{G12C}$ nanoparticles by 20% and 15% in H2030 and H2122 cell lines, respectively, perhaps indicating that there are other non-EGFR-dependent properties of the aptamers that confer increased binding to these NSCLC cell lines.

We next examined the ability of $EGFR_{apt}$-3WJ-si$KRAS^{G12C}$ nanoparticles to silence the expression of $KRAS^{G12C}$ in H2030 and H2122 cells, and used *KRAS* wild-type H1299 NSCLC cells as a negative control. To optimize the dose of pRNA for *in vitro* treatment, we treated H2122 and H2030 cells with increasing doses of $EGFR_{apt}$-3WJ-si$KRAS^{G12C}$ pRNA nanoparticles for 48 h. We found that KRAS expression was suppressed in a dose-dependent manner, with 50 nM of pRNA nanoparticle serving as the lowest, most effective dose (Figure S2). To further

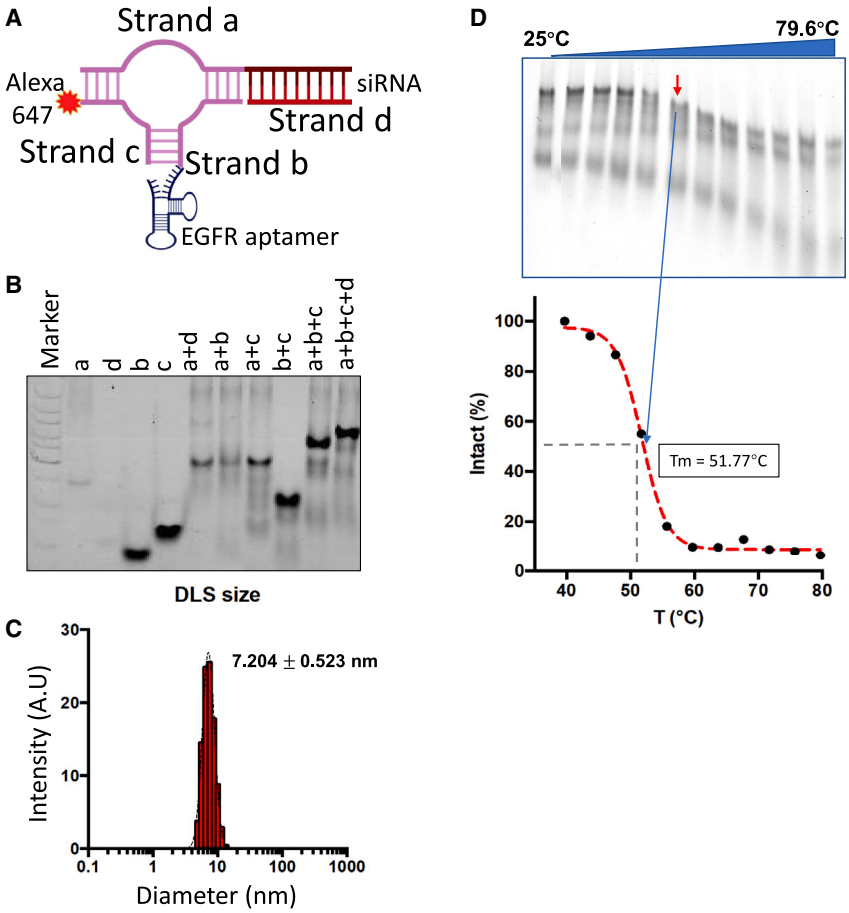

Figure 1. Construction and characterization of EGFR$_{apt}$-3WJ-si*KRAS*^{G12C} pRNA nanoparticles

(A) Schematic of Alexa 647-labeled EGFR$_{apt}$-3WJ-si*KRAS*^{G12C} pRNA structure. (B) Native PAGE showing stepwise assembly of EGFR$_{apt}$-3WJ-si*KRAS*^{G12C} pRNA nanoparticles. (C) DLS assay to assess hydrodynamic size of EGFR$_{apt}$-3WJ-si*KRAS*^{G12C} pRNA nanoparticles. (D) TGGE assay determined T_m value of EGFR$_{apt}$-3WJ-si*KRAS*^{G12C} pRNA nanoparticles.

determine the optimal pRNA treatment time, we treated H2122 and H2030 cells with 50 nM of EGFR$_{apt}$-3WJ-si*KRAS*^{G12C} pRNA nanoparticles and collected cells at various time points after treatment. We found that KRAS mRNA knockdown efficacy is approximately equivalent between 48 and 72 h after treatment with 50 nM of pRNAs, with slightly improved efficacy over 24 h (Figure S2). Thus, in this study, we chose 50 nM of pRNAs for 48 h as the optimal treatment conditions for functional assays. Sanger sequencing of *KRAS* exon 2 was performed to confirm *KRAS* mutation status in all of these cell lines, with H2122 and H2030 harboring homozygous *KRAS*^{G12C} mutations as expected (Figure S3). Then, we treated H2122 and H2030 cells with 50 nM of EGFR$_{apt}$-3WJ-si*KRAS*^{G12C} nanoparticles along with control RNPs (PBS, EGFR$_{apt}$-3WJ-siScramble, and 3WJ-si*KRAS*^{G12C}) for 48 h. We found that 3WJ-si*KRAS*^{G12C} nanoparticles significantly suppressed *KRAS* mRNA expression in *KRAS* mutant cells, and that EGFR aptamer-conjugated EGFR$_{apt}$-3WJ-si*KRAS*^{G12C} nanoparticles significantly further suppressed *KRAS* expression in *KRAS*^{G12C} NSCLCL cell lines (Figure 2C). However, neither 3WJ-si*KRAS*^{G12C} or EGFRapt-3WJ-si*KRAS*^{G12C} nanoparticles were able to significantly decrease *KRAS* expression in *KRAS* wild-type H1299 cells (Figure S4, top panel). Furthermore, by immunoblotting we confirmed that EGFR$_{apt}$-3WJ-si*KRAS*^{G12C} nanoparticles suppressed protein expression of *KRAS* and activation of its downstream signaling components p-MEK-1/2, p-ERK-1/2 in *KRAS*^{G12C} NSCLC cells (Figure 2D), but not *KRAS* wild-type NSCLC cells (Figure S4, bottom panel). These data demonstrated that EGFR$_{apt}$-3WJ-si*KRAS*^{G12C} nanoparticles efficiently silence *KRAS*^{G12C} expression only in *KRAS*^{G12C} mutant NSCLC cells.

EGFR$_{apt}$-3WJ-si*KRAS*^{G12C} nanoparticles suppress KRAS activity, cell growth, migration, and invasion capabilities of NSCLC cells

To investigate whether *KRAS*^{G12C}-specific knockdown might result in reduced KRAS activity, we treated H2122 and H2030 cells with 50 nM of EGFR$_{apt}$-3WJ-si*KRAS*^{G12C} nanoparticles along with control RNPs (PBS, EGFR$_{apt}$-3WJ-siScramble, and 3WJ-si*KRAS*^{G12C}) for 24 h followed by assessment of KRAS functional activation. In both cell lines, we confirmed that 3WJ-si*KRAS*^{G12C} can suppress KRAS activity, which was maximal when cells were treated with EGFR$_{apt}$-3WJ-si*KRAS*^{G12C} nanoparticles (Figure 3A), which is consistent with immunoblotting data showing that EGFR$_{apt}$-3WJ-si*KRAS*^{G12C} nanoparticles suppressed activation of MEK-1/2 and ERK-1.2 (Figure 2D).

Oncogenic KRAS results in persistent stimulation of its downstream signaling intermediates, which results in many of the phenotypic hallmarks of cancer including increased proliferation and metastasis. To assess the effects of depletion of oncogenic *KRAS*^{G12C} by siRNA delivered our RNPs on cell growth, IncuCyte cell proliferation assays were carried out. As shown in Figure 3B, 3WJ-si*KRAS*^{G12C} nanoparticles suppressed NSCLC cell growth, and the presence of EGFR aptamer maximally suppressed cell growth, while the control (scrambled) siRNA RNPs had no effect on cell proliferation. To investigate the influence of *KRAS*^{G12C} knockdown on NSCLC cell metastasis, migration ability, and invasion ability were evaluated by transwell assay and Matrigel assay, respectively. As shown in Figures 3C and S5 (top panels), the number of cells that migrated or invaded into the lower chamber decreased significantly in cells treated with EGFR$_{apt}$-3WJ-si*KRAS*^{G12C} nanoparticles compared with the control siRNA group. The calculated invasion index also confirmed that *KRAS* knockdown decreased cell invasion ability independent of differences in migration (Figure 3C, bottom panels).

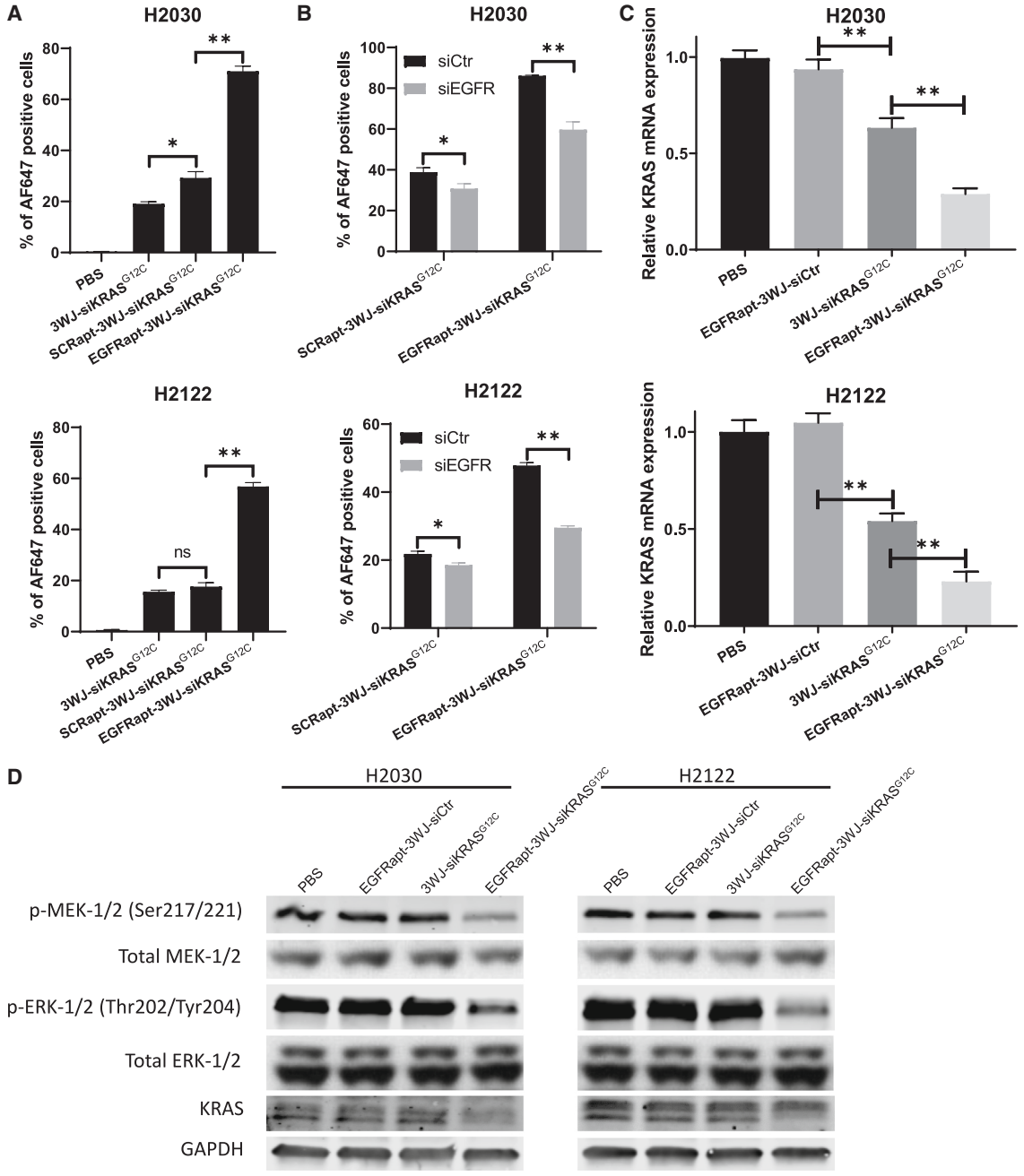

Figure 2. EGFR$_{apt}$-3WJ-si*KRAS*^{G12C} pRNA nanoparticles target EGFR-expressing cells and suppress KRAS expression in human lung cancer

(A and B) Cellular uptake of AF647-labeled pRNA nanoparticles after 1 h incubation was determined by flow cytometry assay. (C) *KRAS* mRNA expression was quantified by qRT-PCR assay 48 h post-treatment with pRNA nanoparticles. (D) KRAS protein expression and activation status of KRAS downstream pathway intermediates was assessed by immunoblotting assay 48 h post-treatment with pRNA nanoparticles. Error bars represent SD. Significance was calculated using Student's t test: **p < 0.001.

EGFR$_{apt}$-3WJ-si*KRAS*^{G12C} nanoparticles sensitize NSCLC cells to chemotherapy and radiation therapy *in vitro*

It has been well documented that hyperactivation of KRAS can lead to development of intrinsic chemotherapy and radiation therapy resistance in tumor cells.[19,20,23] To test whether KRAS suppression by EGFR$_{apt}$-3WJ-si*KRAS*^{G12C} nanoparticles sensitizes NSCLC to radiation therapy, we performed radiation clonogenic assays using 2 Gy ionizing radiation in H2122 and H2030 cell lines at 24 h after pRNA nanoparticle treatment. As shown in Figure 4A, 3WJ-si*KRAS*^{G12C} nanoparticles significantly sensitized cells to radiation treatment, as observed by lower

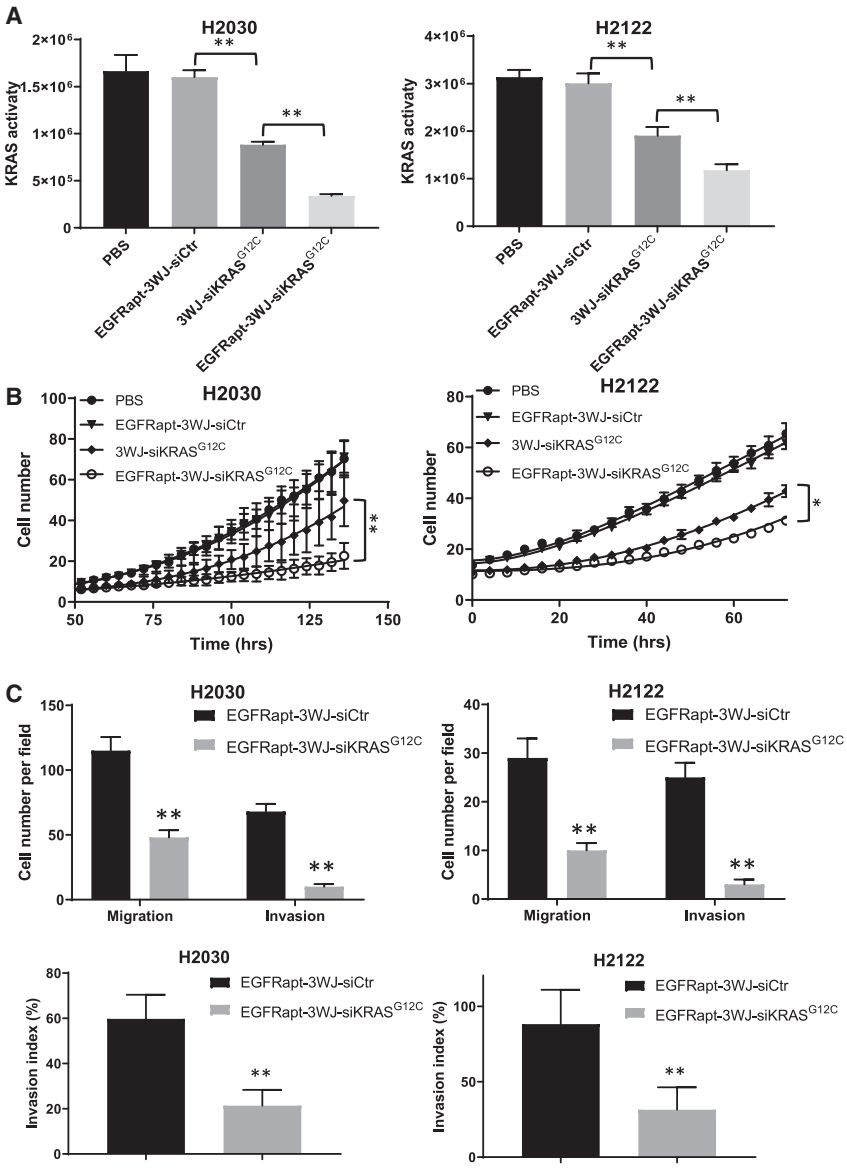

Figure 3. Silencing of *KRAS* by EGFR$_{apt}$-3WJ-si*KRAS*^{G12C} pRNA nanoparticles suppressed KRAS activity, cell growth, and metastatic capabilities of NSCLC cells

(A) KRAS activity was determined by KRAS activation ELISA assay on H2030 and H2122 cells. (B) Effects of KRAS silencing by pRNA nanoparticles on cell growth was determined by IncuCyte cell proliferation assay (cell number reflects percent confluency). (C) Quantification of transwell migration and invasion assays (top panels) and calculated invasion index (bottom panels). Error bars represent SD. Significance (A and C) was calculated using Student's t test; significance (B) was calculated using one-way ANOVA analysis followed by Tukey's post-hoc test: *p < 0.05, **p < 0.001.

cell surviving fraction after 2 Gy compared with treatment with pRNA nanoparticles containing control siRNA. EGFR$_{apt}$-3WJ-si*KRAS*^{G12C} nanoparticles further sensitized NSCLC cells to radiation therapy. We further investigated whether EGFR$_{apt}$-3WJ-si*KRAS*^{G12C} nanoparticles could sensitize cells to cisplatin, a common first-line chemotherapy drug for NSCLC. Cells were pretreated with EGFR$_{apt}$-3WJ-si*KRAS*^{G12C} nanoparticles for 24 h, followed by 72 h cisplatin treatment. alamarBlue cytotoxicity assays were used to determine whether the RNPs could alter the half-maximal inhibitory concentration (IC_{50}) values to cisplatin. As shown in Figure 4B, EGFR$_{apt}$-3WJ-si*KRAS*^{G12C} nanoparticles significantly lowered the IC_{50} values to cisplatin compared with control siRNA RNPs, decreasing from 7.6 to 3.8 μM and 6.6 to 1.3 μM in H2030 and H2122 cell lines, respectively. This finding was corroborated by clonogenic assays (Figure 4C), revealing reduced cell surviving fraction in both cell lines during treatment with increasing doses of cisplatin and EGFR$_{apt}$-3WJ-si*KRAS*^{G12C} nanoparticles. Together, these data support that *KRAS* mutation-specific silencing by EGFR$_{apt}$-3WJ-si*KRAS*^{G12C} nanoparticles sensitizes NSCLC cells to chemoradiation therapy *in vitro*.

EGFR$_{apt}$-3WJ-si*KRAS*^{G12C} nanoparticles are preferentially taken up by tumors and significantly attenuate tumor growth *in vivo*

We further investigated the potential therapeutic effects of EGFR$_{apt}$-3WJ-si*KRAS*^{G12C} nanoparticles *in vivo*. First, to determine the *in vivo* siRNA delivery effects of EGFR$_{apt}$-3WJ-si*KRAS*^{G12C} nanoparticles, we established heterotopic tumor xenografts with H2122 cells in nude mice. To decrease phototoxicity, we conjugated pRNA nanoparticles with Alexa 750, and systemically delivered Alexa 750-conjugated pRNA nanoparticles in TES via tail vein injection. At 24 h post-injection, an IVIS lumina imaging system was utilized to assess pRNA biodistribution in live animals and in *ex vivo* organs. Live imaging demonstrated that Alexa 750-conjugated 3WJ-si*KRAS*^{G12C} nanoparticles exhibited intense fluorescence in the areas of the tumors, and the presence of EGFR aptamer further increased the accumulation of RNPs in the tumor (Figure 5A, left top). Furthermore, *ex vivo* organ biodistribution analysis confirmed that EGFR aptamer facilitated pRNA nanoparticle accumulation in the tumors, with minimal uptake in some normal organs including lung, spleen, and heart (Figure 5A, left bottom). We also compared the *in vivo* biodistribution of EGFR$_{apt}$-3WJ-si*KRAS*^{G12C} and SCR$_{apt}$-3WJ-si*KRAS*^{G12C} pRNA nanoparticles. As shown in Figure S6, EGFRapt-pRNA can more efficiently accumulate in tumor xenografts compared with SCRapt-pRNA. To identify the optimal dose of RNPs for *in vivo* treatment, serial doses of EGFR$_{apt}$-3WJ-si*KRAS*^{G12C} nanoparticles were intravenously administered to mice bearing H2122

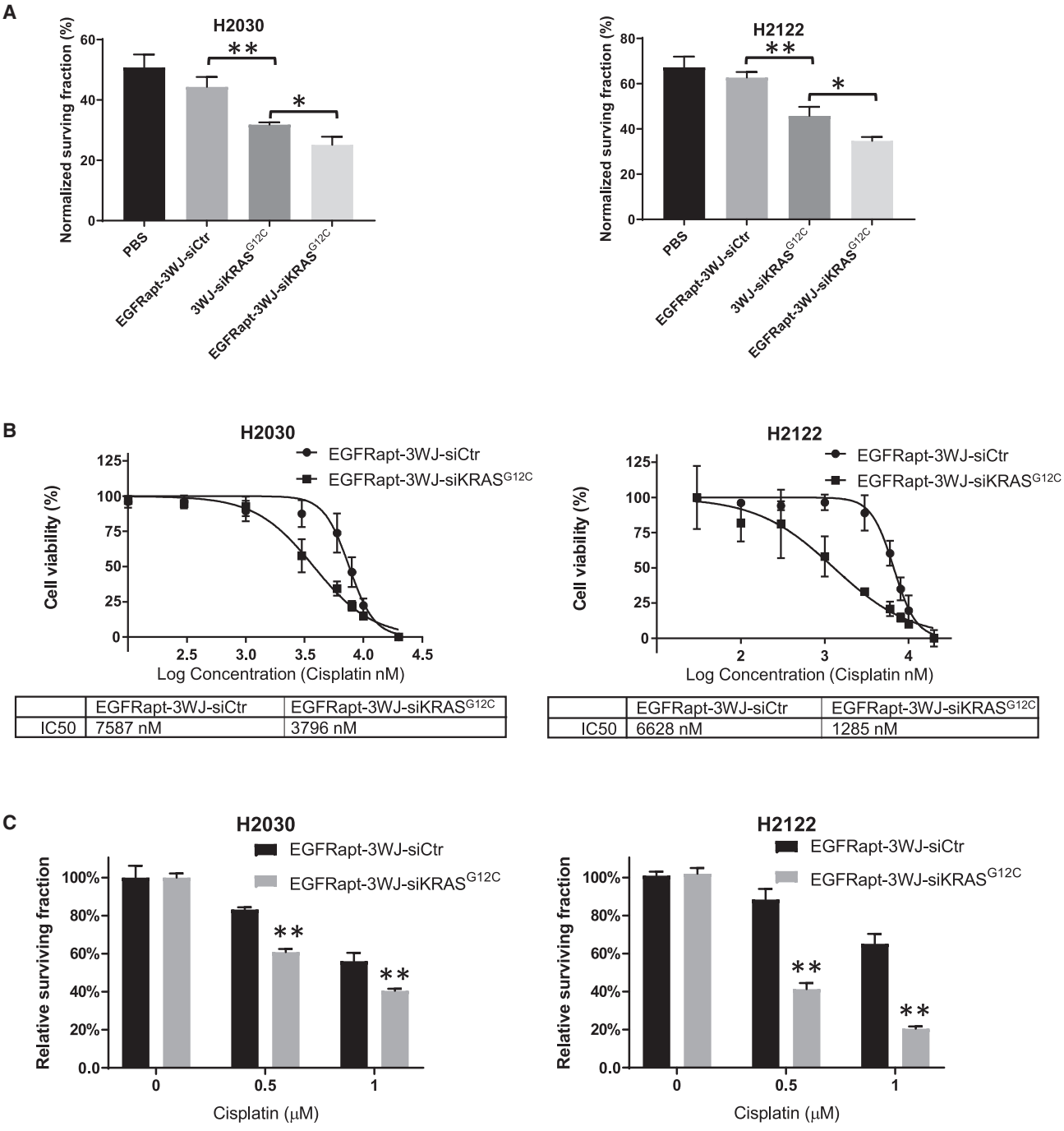

	EGFRapt-3WJ-siCtr	EGFRapt-3WJ-siKRAS^{G12C}
IC50	7587 nM	3796 nM

	EGFRapt-3WJ-siCtr	EGFRapt-3WJ-siKRAS^{G12C}
IC50	6628 nM	1285 nM

Figure 4. EGFR$_{apt}$-3WJ-si*KRAS*^{G12C} pRNA nanoparticles sensitized NSCLC cells to radiotherapy and chemotherapy

(A) Radiation clonogenic assay was performed and normalized surviving fraction was calculated to evaluate sensitivity of NSCLC cells to radiation treatment after 48 h pRNA treatment. (B and C) Effects of 48 h treatment of EGFR$_{apt}$-3WJ-si*KRAS*^{G12C} pRNA nanoparticles on cisplatin cytotoxicity on NSCLC cells assessed by both alamarBlue (B) and colony formation assays (C). Error bars represent SD. Significance was calculated using Student's t test: *$p < 0.05$, **$p < 0.001$.

xenografts every 2 days, four times over 7 days, and tumors were isolated for extraction of total RNA and protein (Figure 5B). We found that *KRAS* RNA (Figure 5C) and ERK activation (Figure 5D) were suppressed in a dose-dependent manner. One micromole per kilogram dose (1 μmol/kg) of pRNA nanoparticle was the most effective dose for suppression of *KRAS in vivo*. To assess whether systemically

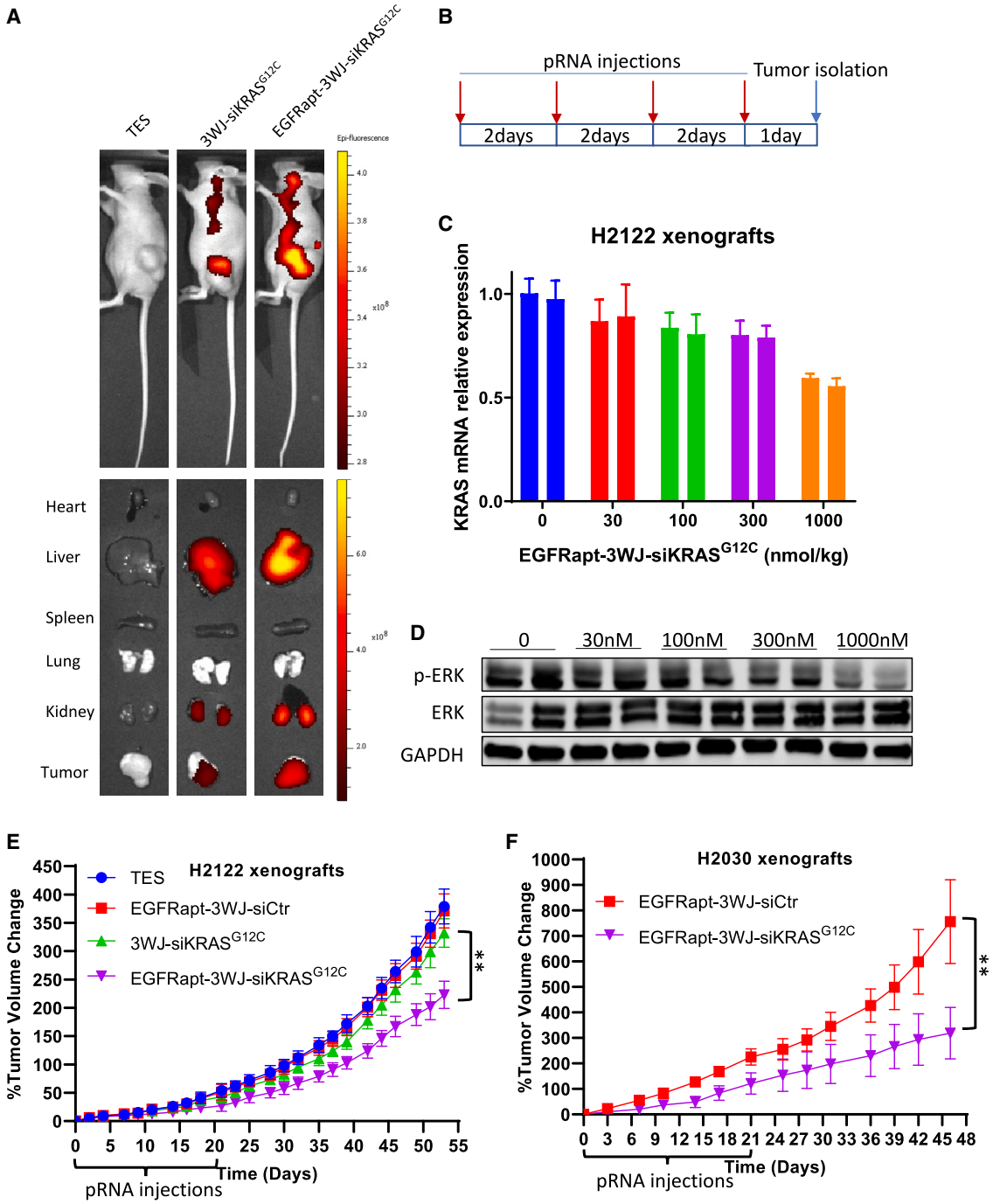

Figure 5. *In vivo* evaluation of EGFR$_{apt}$-3WJ-si*KRAS*^{G12C} pRNA nanoparticles on NSCLC tumor xenograft models

(A) IVIS lumina imaging system was used to study the biodistribution of Alexa 750-labeled EGFR$_{apt}$-3WJ-si*KRAS*^{G12C} pRNA nanoparticles in live mice (top panels) and dissected organs *ex vivo* (bottom panels). (B) Dosing schematic of pRNA nanoparticle injection and tumor isolation for dose optimization study. (C and D) After four intravenous administrations of increasing doses of EGFR$_{apt}$-3WJ-si*KRAS*^{G12C} pRNA nanoparticles, *KRAS* mRNA expression (C) in tumor xenografts was quantified by qRT-PCR, and activation status of KRAS downstream MAPK pathway signaling was evaluated by p-ERK immunoblotting (D). (E and F) Tumor growth curve of H2122 and H2030 xenograft mouse models, which were treated with pRNA nanoparticles two times a week for 3 weeks (n = 10 mice per group). Error bars represent SEM. Significance was calculated using one-way ANOVA analysis followed by Tukey's post-hoc test: **$p < 0.001$.

delivered $EGFR_{apt}$-3WJ-si$KRAS^{G12C}$ nanoparticles could suppress tumor growth, mice bearing H2122 or H2030 tumors were injected with 1 μmol/kg of the indicated pRNA nanoparticles twice a week for 3 weeks. We noted suppression of tumor growth with $EGFR_{apt}$-3WJ-si$KRAS^{G12C}$, but not 3WJ-si$KRAS^{G12C}$ nanoparticles (Figures 5E and 5F). These data confirm that $EGFR_{apt}$-3WJ-si$KRAS^{G12C}$ nanoparticles are more effective RNPs for targeting $KRAS^{G12C}$ NSCLC cells *in vivo* relative to 3WJ-si$KRAS^{G12C}$ RNPs, in alignment with the results obtained from our *in vitro* cell-based experiments.

DISCUSSION

For more than 30 years, development of effective therapeutics targeting oncogenic RAS has eluded the field and RAS was thought to be "undruggable."[27] Although breakthroughs have been made recently with the development of covalent inhibitors targeting $KRAS^{G12C}$, such as AMG510 (sotorasib), there are still challenges and questions regarding the development and prevention of drug resistance, and the ability to successfully target other KRAS mutations.[27] Other strategies targeting KRAS have been attempted. For example, systemic delivery of *KRAS* siRNA in nanoparticles suppressed pancreatic, lung, and colorectal cancer xenografts in various mouse models.[35–38] SiG12D-LODER, is a specific siRNA targeting $KRAS^{G12D}$, and is in a phase II trial to evaluate the clinical efficacy of siG12D LODER in combination with gemcitabine and nab-paclitaxel in pancreatic cancer patients with $KRAS^{G12D}$ mutation (NCT01676259).[27,39] AZD4785, a chemically modified antisense oligonucleotide, significantly depleted cellular *KRAS* mRNA and protein in a preclinical study,[40] but failed to suppress KRAS expression in patients in a clinical trial (NCT03101839). Further studies are ongoing to improve delivery efficiency, uptake, and internalization to make this approach more effective.

In this study, we took a mutation-specific gene-silencing approach by constructing novel multifunctional $EGFR_{apt}$-3WJ-si$KRAS^{G12C}$ nanoparticles and explored the potential of these RNPs carrying $KRAS^{G12C}$ siRNA to target *KRAS* in NSCLC cells in a mutation-specific fashion. Furthermore, we added $EGFR_{apt}$ to the RNP to enhance tumor cell targeting. Our results demonstrate that $EGFR_{apt}$-3WJ-si$KRAS^{G12C}$ nanoparticles were successfully delivered to (and enriched in) NSCLC cells both *in vitro* and *in vivo*. These RNA nanoparticles effectively silenced *KRAS* expression only in $KRAS^{G12C}$ mutant cells, attenuated activation of the MAPK signaling pathway, suppressed cancer cell migration and invasion properties, enhanced chemotherapy and radiotherapy sensitivity, and showed some tumor growth inhibitor properties in tumor xenograft mouse models.

Currently, a variety of nanocarriers are being investigated for siRNA delivery, such as polymers, dendrimers, liposomes, exosomes, and RNA nanoparticles.[28,32,41–43] Among them, 3WJ pRNA nanoparticles are showing great potential as an efficient siRNA delivery system, harnessing beneficial characteristics, which include a relatively uniform nanoscale size, precise stoichiometry, ultrastability, and a high degree of biocompatibility compared with other therapeutics (e.g., liposomal nanoparticles). In addition, the branches/arms of the 3WJ motif could be easily modified with different subunits, such as multiple sequence-independent siRNAs, different RNA aptamers to improve specificity, or fluorescent dyes, without disrupting the stability and conformation.[29] This technology enables multiple functional units for targeting, therapy, and tracking, which can all be combined into one nanoparticle. In our study, $EGFR_{apt}$-3WJ-si$KRAS^{G12C}$ nanoparticles are ultracompact with 7.2 + 0.5 nm diameter, and thermostable with a T_m of 51.77°C. Alexfluo647 was conjugated the RNP to form Alexa 647-$EGFR_{apt}$-3WJ-si$KRAS^{G12C}$ nanoparticles for *in vitro* cellular binding and *in vivo* biodistribution analysis. Alternatively, multiple units of the same function, such as different siRNAs targeting the same gene or different genes, can be combined on the same 3WJ pRNA nanoparticle for enhanced therapeutic effects. For example, as resistance to AMG510 has been shown to be associated with intratumoral heterogeneity and evolution of new non-*G12C* mutations,[44] one could envision putting on multiple mutation-specific siRNAs targeting *KRAS G12C*, *G12D*, *G12R*, *G12V*, etc., to suppress development of resistance to these RNPs. Conversely, we could fashion these $EGFR_{apt}$-3WJ-si$KRAS^{G12C}$ nanoparticles to be more efficient at suppressing $KRAS^{G12C}$ activity by adding another $KRAS^{G12C}$ siRNA on another branch of 3WJ pRNA to increase dose of gene silencing.

Overexpression of EGFR has been reported in many human malignancies and is detected in up to 85% in NSCLC patients.[33,45] EGFR monoclonal antibodies including cetuximab and necitumumab have been used to treat NSCLC patients combined with cytotoxic chemotherapeutics.[46] Recently, RNA aptamers are emerging as promising targeting moieties, analogous to monoclonal antibodies. EGFR aptamers are selected through SELEX methods (systematic evolution of ligands by exponential enrichment), and have been utilized to decorate nanocarriers for more targeted delivery.[34,43] In our study, the addition of $EGFR_{apt}$ to 3WJ-si$KRAS^{G12C}$ showed obvious enhancement on cellular uptake and gene knockdown in both *in vitro* and *in vivo* experiments. Although EGFR depletion by *EGFR* siRNA did not completely abolish $EGFR_{apt}$ pRNA binding (Figure 2B), this observation might be due to insufficient *EGFR* knockdown or, more likely, that $EGFR_{apt}$ may nonspecifically bind to the membrane or other membrane receptors/components. This represents an opportunity to further optimize $EGFR_{apt}$ binding specificity in the future through re-engineering of $EGFR_{apt}$ or utilizing other targeting moieties.

Upregulation of KRAS-mediated signaling pathways is one of the mechanisms of chemotherapy resistance. For example, KRAS mutations have been shown to activate the anti-oxidant NRF2 pathway in NSCLC, thereby decreasing cisplatin-induced reactive oxygen species within the tumor cells, ultimately leading to cisplatin resistance.[47] Studies have also shown that KRAS mutations render patients resistant to gefitinib in NSCLC and cetuximab resistance in colorectal cancer.[48,49] In addition, KRAS mutations are also associated with radiation resistance in various cancers, including NSCLC and colorectal cancer.[22,23] Herein, we document that $EGFR_{apt}$-3WJ-si$KRAS^{G12C}$ nanoparticles can sensitize NSCLC cells to radiation therapy or the first-line chemotherapy agent cisplatin (Figure 4). The results show the potential of 3WJ RNPs for allowing reduction in the doses of

chemotherapy or radiotherapy leading to reduced normal tissue toxicity or, conversely, allowing enhancement of therapeutic efficacy if doses are kept the same.

In conclusion, we have demonstrated that $EGFR_{apt}$-3WJ-si$KRAS^{G12C}$ RNPs efficiently suppressed *KRAS* mRNA expression, resulting in suppression of downstream effector pathways in $KRAS^{G12C}$ NSCLC cells, leading to suppression of tumor cell proliferation, migration/invasion ability, and sensitized NSCLC cells to chemoradiotherapy. Furthermore, our animal modeling showed excellent biodistribution of the RNPs to the tumor, effective *KRAS* silencing, and subsequent tumor growth inhibition. In addition, the 3WJ pRNA motif is universal and can be easily applied to target other *KRAS* mutant variants. Overall, these data support that 3WJ pRNA is an attractive RNA nanotechnology platform to deliver *KRAS* mutation-specific siRNA for the treatment of *KRAS*-driven human cancers that could lead to a widened therapeutic index by being a more tumor-selective therapy.

MATERIALS AND METHODS

Construction of $EGFR_{apt}$-3WJ-si$KRAS^{G12C}$ RNA nanoparticles

Multifunctional 3WJ pRNA nanoparticles (RNPs) were prepared using a bottom-up self-assembly approach as described previously.[50–52] The $EGFR_{apt}$-3WJ-Alexa647-si$KRAS^{G12C}$ consisted of four components attached to the 3WJ core motif (Figure 1A), harboring EGFR-targeting RNA aptamer ($EGFR_{apt}$) as a targeting ligand; Alexa Fluor 647 or 750 (Thermo Fisher Scientific, Waltham, MA) as a fluorescent imaging module; a $KRAS^{G12C}$ sense strand, and a $KRAS^{G12C}$ anti-sense strand, as the therapeutic module. The controls include RNPs without targeting $EGFR_{apt}$ ligand (denoted as 3WJ-si$KRAS^{G12C}$), with scramble aptamer ligand (denoted as SCRapt-3WJ-si$KRAS^{G12C}$), without therapeutic module (denoted as $EGFR_{apt}$-3WJ-siScramble), or without therapeutic and targeting modules (denoted as 3WJ). The sequences of the four strands of $EGFR_{apt}$-3WJ-si$KRAS^{G12C}$ RNPs are as below: strand "a" (5′-UUG CCA UGU GUA UGU GGG AGU UGG AGC UUG UGG CGU AGU U-3′), strand "b" (5′-CCC ACA UAC UUU GUU GAU CC-$EGFR_{apt}$-3′), strand "c" (5′-GGA UCA AUC AUG GCA A-3′), strand "d" (5′-CUA CGC CAC AAG CUC CAA C-3′). The complete pRNA sequences are provided in Table S1. The $KRAS^{G12C}$ siRNA sequence is derived from a previous publication that demonstrated that this sequence could knockdown oncogenic *KRAS* but not wild-type *KRAS*.[53] The RNA fragments were either synthesized via standard phosphoramidite chemistry by ourselves, or purchased from Trilink (San Diego, CA), and strands a, b, and c are 2′-F modified at cytosine (C) and uracil (U) nucleotides to make the RNPs resistant to RNase degradation. For the experiments involving the detection of RNPs (binding assay), strand c was conjugated to fluorophore Alexa 647 at the 3′ end. The RNP was formed through one-step self-assembly by mixing the four RNA module strands at equal molar ratios in annealing buffer (10 mM Tris [pH 7.5–8.0], 50 mM NaCl, 1 mM EDTA) and heated to 95°C for 5 min and slowly cooled to 4°C over 45 min. Stepwise assembly of RNPs was verified on a native 10% PAGE running in 1× TBE buffer (89 mM Tris-borate, 2 mM EDTA), and imaged by Typhoon FLA7000 (GE Healthcare) under the ethidium bromide channel. The self-assembled $EGFR_{apt}$-3WJ-Alexa647-si$KRAS^{G12C}$ RNPs were purified from 8 M urea-containing PAGE and stored at −80°C until use. The RNPs were freshly reconstituted in PBS before each use.

Characterization of the assembled pRNA-3WJ nanoparticle

The molecular size of assembled 3WJ pRNA nanoparticles was confirmed by native 10% PAGE gel electrophoresis. The hydrodynamic diameter of pRNA nanoparticles was assessed by DLS using a Zetasizer nano ZS (Malvern Instruments) at 25°C via a laser wavelength at 633 nm. The thermodynamic stability of the pRNA nanoparticles was studied using the TGGE system (Biometra, Germany), as described previously. The apparent T_m of the pRNA nanoparticle was determined as the temperature at which 50% of the pRNA nanoparticle remained assembled. Data shown are representative of three independent measurements.

Cell culture, chemicals, and antibodies

Human NSCLC cell lines H2122, H2030, and H1299 were obtained from the American Type Culture Collection (ATCC) and maintained in RPMI 1640 medium (Thermo Fisher Scientific), with 10% FBS (GE Healthcare, Chicago, IL) and 1% penicillin/streptomycin (Life Technologies, Carlsbad, CA). Cells were cultured in 37°C with 5% CO_2. Typically, cells were kept in culture for a minimum of two passages prior to and a maximum of 20 passages during experiments. The identity of all cell lines was confirmed by STR genotyping (Identifier Kit, Applied Biosystems, Carlsbad, CA). For the detection of mycoplasma in cell culture, the Universal Mycoplasma Detection Kit (ATCC) was used. Cisplatin (Sigma, St. Louis, MO) was dissolved in dimethyl formamide (Sigma). Anti-KRAS antibody was purchased from Santa Cruz Biotechnology (Dallas, TX); anti-p-MEK-1/2, p-ERK-1/2, EGFR, and GAPDH primary antibodies were purchased from Cell Signaling Technology (Danvers, MA). Anti-rabbit and anti-mouse secondary antibodies were purchased from Li-Cor Bioscience (Lincoln, NE).

DNA extraction and *KRAS* mutation analysis

Genomic DNA was isolated by using a QIAamp DNA mini kit (QIAGEN) according to the manufacturer's instructions. Exon 2 of *KRAS* gene was amplified by polymerase chain reaction (PCR) using the following primers: forward 5-TGA CAT GTT CTA ATA TAG TCA G-3 and reverse: 5-ACA AGA TTT ACC TCT ATT GTT G-3. PCR was performed as described previously.[23] PCR products were purified using a DNA purification kit (Zymo Research, Irvine, CA) and direct Sanger sequencing was performed on capillary electrophoresis using an Applied Biosystems 3730 DNA Analyzer (Thermo Fisher Scientific).

In vitro pRNA nanoparticle cellular binding assay

Specific binding of pRNA nanoparticles to NSCLC cells was assessed *in vitro* by flow cytometry. In brief, 1×10^5 H2122 and H2030 cells were resuspended in 100 μL PBS, and incubated with 50 nM of Alexa 647-labeled $EGFR_{apt}$-3WJ-si$KRAS^{G12C}$ and 3WJ-si$KRAS^{G12C}$ pRNA nanoparticles at 37°C for 1 h. After washing three times with PBS, the cells were subjected to flow cytometry analysis using the BD LSR Fortessa flow cytometer (Becton Dickinson). Data were analyzed

using the FlowJo 7.6.1 software (Tree Star). For EGFR-dependent selectivity assessment, cells were treated with *EGFR*-siRNA to knock down EGFR expression, followed 24 h later by pRNA nanoparticle cellular binding assay. Data shown are representative of three independent experiment.

Real-time qPCR analysis

KRAS gene silencing was detected by real-time quantitative PCR assay. Total cellular RNA was isolated using TRIzol (Thermo Fisher Scientific), and 1 μg of total RNA was reverse-transcribed using SuperScript reverse transcriptase (Bio-Rad). PCR was performed on iCYCLER real-time PCR machine (Bio-Rad) using SYBR Green chemistry (Bio-Rad). The genes expression levels were normalized to housekeeping gene *GAPDH*. The primer sequences are as follows: *KRAS* forward: 5′-GAC TCT GAA GAT GTA CCT ATG GTC CTA-3′ and reverse: 5′-CAT CAT CAA CAC CCT GTC TTG TC-3′; *GAPDH* forward: 5′-AAC GGG AAG CTT GTC ATC AAT GGA AA-3′ and reverse: 5′-GCA TCA GCA GAG GGG GCA GAG-3′. Experiments were performed three times.

Immunoblotting

Immunoblotting was performed as described previously.[54] In brief, cell lysates were prepared using RIPA buffer (Thermo Fisher Scientific) supplemented with 1× protease inhibitors (Complete, Roche, Indianapolis, IN) and phosphatase inhibitors (PhosSTOP, Roche) followed by protein quantification with the DC protein assay kit (Bio-Rad, Hercules, CA). Equal amounts of protein were loaded and resolved by sodium dodecyl sulfate-polyacrylamide gel electrophoresis and transferred onto nitrocellulose membranes. Membranes were incubated in 5% bovine serum albumin in Tris-buffered saline with 0.1% Tween 20 (TBST) blocking buffer for 1 h at room temperature. Primary antibodies with dilution of 1:200–1,000 were allowed to bind overnight at 4°C, or for 2 h at room temperature. After washing in TBST, the membranes were incubated with immunofluorescent secondary antibodies at a 1:5,000 dilution for 1 h at room temperature. Membranes were washed with TBST and allowed to air dry prior to imaging via Li-Cor Odyssey CLx Imaging System (Thermo Fisher Scientific). Immunoblotting data represent three independent experiments.

KRAS activity assay

As previous reported,[23] KRAS activity was detected using a Ras Activation ELISA assay kit (Millipore) according to the manufacturer's instructions. GST-Raf-RBD was used to pull down RAS-GTP from 50 μg of cell lysate prepared the same way as for immunoblotting, and then a primary antibody for KRAS was added, followed by incubation with an HRP-conjugated secondary antibody. After addition of developing reagent, chemiluminescent reaction was determined with a Fluoroskan Ascent FL luminometer. Experiments were repeated three times.

IncuCyte cell proliferation assay

Cells were treated with various pRNA nanoparticles accordingly for 48 h, and then seeded at 1,000–2,000 cells per well in 96-well plates. Cell confluence as a measure of cell growth over time was monitored every 4 h for up to 6 days using the IncuCyte ZOOM Live-Cell Imaging System (Essen Biosciences) until cells reached about 80% confluence. Cell proliferation curves were plotted using GraphPad Prism v.9.0 for Windows (La Jolla, CA). Experiments were repeated three times.

Cell migration and invasion assays

In the migration assay, cells were treated for 48 h with nanoparticles, then 2×10^4 cells were resuspended in 300 μL cell culture medium with 0.5% FBS and placed in the upper transwell chamber (8 μm pore size, BD Biosciences). The upper chamber was placed in a 24-well culture dish containing 1 mL of complete cell culture medium (with 10% FBS). After 48 h incubation, non-migrated cells on the upper membrane were removed with a cotton swab. Migrated cells on the bottom surface were fixed with methanol (−20°C) and stained with 0.5% crystal violet. Four fields of each well were photographed, and the cells were counted. In the invasion assay, Matrigel-coated transwell chambers (BD Biosciences) were used. Percentage invasion was calculated as the number of invaded cells in comparison with the number of migrated cells. All experiments were repeated three times.

Chemotherapy and radiation sensitivity assays

To study the effects of pRNA nanoparticles on chemoradiation sensitivity in NSCLC, a clonogenic assay was performed as reported previously.[23] In brief, cells were treated with the indicated pRNA nanoparticles for 24 h, and then harvested to generate a single-cell suspension and seeded onto 60-mm tissue culture plates in triplicate. After 24 h, for the radiation sensitivity assay, cells were irradiated with 0 or 2 Gy X-rays using a Radsource RS2000 biological irradiator (RadSource, GA). For the chemotherapy sensitivity assay, cells were treated with increasing doses of cisplatin (0, 0.5, and 1 μM). Twenty-four hours later, the medium was changed to remove cisplatin. Ten to 14 days after irradiation or cisplatin treatment, colonies were fixed with methanol/acetic acid, stained with 0.5% crystal violet, and the numbers of colony-forming units containing at least 50 cells were counted using a dissecting microscope (Leica Microsystems, Buffalo Grove, IL) and surviving fractions were calculated. Experiments were performed three independent times.

Cisplatin cytotoxicity was also assessed by alamarBlue assay (Bio-Rad). In brief, cells were treated with pRNA nanoparticles as indicated for 24 h, and then collected and seeded in 96-well plates in 4 replicates at a density of 2,000 cells per well in 100 μL medium. The next day (∼48 h after adding pRNA), cells were treated with cisplatin at various concentrations. After 72 h, alamarBlue reagent was added to cells at 37°C for 4 h, and absorbance was measured at 490 nm. IC_{50} was determined using the nonlinear four-parameter regression function in GraphPad Prism. Experiments were performed three independent times.

Biodistribution and antitumor activity of pRNA nanoparticles *in vivo*

Animal studies were conducted in accordance with an approved protocol adhering to the IACUC policies and procedures at The Ohio State University. Six- to 8-week-old male athymic nude mice (Taconic

Farms, NY) were caged in groups of five or less and fed with a diet of animal chow and water *ad libitum*. H2122 and H2030 cells were injected subcutaneously into the flanks of each mouse at 5×10^6 cells per injection. When the tumor size reached 150–200 mm^3, the mice were randomly divided into 4 groups with 10 mice per group and injected with pRNA nanoparticles via tail vein twice a week for 3 weeks. The tumor volume was monitored 3 times a week, and tumor size was calculated using the formula: $V = \frac{L \times W^2}{2}$, where V (volume) is determined by length (L) and width (W). For *in vivo* pRNA nanoparticle targeting and tumor imaging, mice were tail vein injected with 100 μL of 20 μM of RNA Alexa 750-labeled pRNA nanoparticles, and animal or tissue were imaged using the IVIS lumina imaging system with Living Images 3.0 software (Caliper Life Sciences).

Data analysis

Data are presented as the mean ± standard deviation (SD) or standard error of the mean (SEM), with a representative experiment from at least three independent experiments shown. The difference among groups was calculated using Student's t test or one-way ANOVA analysis followed by Tukey's post-hoc test (GraphPad Prism).

DATA AND CODE AVAILABILITY

All data needed to evaluate the conclusions in the paper are present in the paper and/or the supplemental information. Additional data related to this paper may be requested from the authors.

SUPPLEMENTAL INFORMATION

Supplemental information can be found online at https://doi.org/10.1016/j.omtn.2023.07.027.

ACKNOWLEDGMENTS

This work was supported by the following grants: The Ohio State University Comprehensive Cancer Center (OSU-CCC) National Institutes of Health (P30 CA016058), and American Cancer Society RSG-17-221-01-TBG (to T.M.W.).

AUTHOR CONTRIBUTIONS

L.Y., Z.L., P.G., and T.M.W. designed the study, participated in the supervision, and coordination of the study. L.Y., Z.L., and T.M.W. conceived and designed the experiments. L.Y. and Z.L. performed most of the experiments. All authors analyzed the data, contributed to the writing, review, and revision of the manuscript, and read and approved the final manuscript.

DECLARATION OF INTERESTS

P.G. is the consultant of Oxford Nanopore Technologies; the cofounder of Shenzhen P&Z Bio-medical Co. Ltd., as well as the cofounder of ExonanoRNA, LLC, and its subsidiary Weina Biomedical (Guangdong), Ltd.

REFERENCES

1. Bos, J.L. (1989). ras oncogenes in human cancer: a review. Cancer Res. *49*, 4682–4689.
2. Hanahan, D., and Weinberg, R.A. (2011). Hallmarks of cancer: the next generation. Cell *144*, 646–674. https://doi.org/10.1016/j.cell.2011.02.013.
3. Karnoub, A.E., and Weinberg, R.A. (2008). Ras oncogenes: split personalities. Nat. Rev. Mol. Cell Biol. *9*, 517–531. https://doi.org/10.1038/nrm2438.
4. Lito, P., Solomon, M., Li, L.S., Hansen, R., and Rosen, N. (2016). Allele-specific inhibitors inactivate mutant KRAS G12C by a trapping mechanism. Science *351*, 604–608. https://doi.org/10.1126/science.aad6204.
5. Patricelli, M.P., Janes, M.R., Li, L.S., Hansen, R., Peters, U., Kessler, L.V., Chen, Y., Kucharski, J.M., Feng, J., Ely, T., et al. (2016). Selective Inhibition of Oncogenic KRAS Output with Small Molecules Targeting the Inactive State. Cancer Discov. *6*, 316–329. https://doi.org/10.1158/2159-8290.CD-15-1105.
6. Siegel, R.L., Miller, K.D., Fuchs, H.E., and Jemal, A. (2021). Cancer Statistics, 2021. CA A Cancer J. Clin. *71*, 7–33. https://doi.org/10.3322/caac.21654.
7. Clinical Lung Cancer Genome Project CLCGP; Network Genomic Medicine NGM (2013). A genomics-based classification of human lung tumors. Sci. Transl. Med. *5*, 209ra153. https://doi.org/10.1126/scitranslmed.3006802.
8. Dogan, S., Shen, R., Ang, D.C., Johnson, M.L., D'Angelo, S.P., Paik, P.K., Brzostowski, E.B., Riely, G.J., Kris, M.G., Zakowski, M.F., and Ladanyi, M. (2012). Molecular epidemiology of EGFR and KRAS mutations in 3,026 lung adenocarcinomas: higher susceptibility of women to smoking-related KRAS-mutant cancers. Clin. Cancer Res. *18*, 6169–6177. https://doi.org/10.1158/1078-0432.CCR-11-3265.
9. El Osta, B., Behera, M., Kim, S., Berry, L.D., Sica, G., Pillai, R.N., Owonikoko, T.K., Kris, M.G., Johnson, B.E., Kwiatkowski, D.J., et al. (2019). Characteristics and Outcomes of Patients With Metastatic KRAS-Mutant Lung Adenocarcinomas: The Lung Cancer Mutation Consortium Experience. J. Thorac. Oncol. *14*, 876–889. https://doi.org/10.1016/j.jtho.2019.01.020.
10. Scheffler, M., Ihle, M.A., Hein, R., Merkelbach-Bruse, S., Scheel, A.H., Siemanowski, J., Brägelmann, J., Kron, A., Abedpour, N., Ueckeroth, F., et al. (2019). K-ras Mutation Subtypes in NSCLC and Associated Co-occuring Mutations in Other Oncogenic Pathways. J. Thorac. Oncol. *14*, 606–616. https://doi.org/10.1016/j.jtho.2018.12.013.
11. Linardou, H., Dahabreh, I.J., Kanaloupiti, D., Siannis, F., Bafaloukos, D., Kosmidis, P., Papadimitriou, C.A., and Murray, S. (2008). Assessment of somatic k-RAS mutations as a mechanism associated with resistance to EGFR-targeted agents: a systematic review and meta-analysis of studies in advanced non-small-cell lung cancer and metastatic colorectal cancer. Lancet Oncol. *9*, 962–972. https://doi.org/10.1016/S1470-2045(08)70206-7.
12. Mao, C., Qiu, L.X., Liao, R.Y., Du, F.B., Ding, H., Yang, W.C., Li, J., and Chen, Q. (2010). KRAS mutations and resistance to EGFR-TKIs treatment in patients with non-small cell lung cancer: a meta-analysis of 22 studies. Lung Cancer *69*, 272–278. https://doi.org/10.1016/j.lungcan.2009.11.020.
13. Kobayashi, S., Boggon, T.J., Dayaram, T., Jänne, P.A., Kocher, O., Meyerson, M., Johnson, B.E., Eck, M.J., Tenen, D.G., and Halmos, B. (2005). EGFR mutation and resistance of non-small-cell lung cancer to gefitinib. N. Engl. J. Med. *352*, 786–792. https://doi.org/10.1056/NEJMoa044238.
14. Pao, W., Miller, V., Zakowski, M., Doherty, J., Politi, K., Sarkaria, I., Singh, B., Heelan, R., Rusch, V., Fulton, L., et al. (2004). EGF receptor gene mutations are common in lung cancers from "never smokers" and are associated with sensitivity of tumors to gefitinib and erlotinib. Proc. Natl. Acad. Sci. USA *101*, 13306–13311. https://doi.org/10.1073/pnas.0405220101.
15. Jacobs, S.A., Lee, J.J., George, T.J., Wade, J.L., 3rd, Stella, P.J., Wang, D., Sama, A.R., Piette, F., Pogue-Geile, K.L., Kim, R.S., et al. (2021). Neratinib-Plus-Cetuximab in Quadruple-WT (KRAS, NRAS, BRAF, PIK3CA) Metastatic Colorectal Cancer Resistant to Cetuximab or Panitumumab: NSABP FC-7, A Phase Ib Study. Clin. Cancer Res. *27*, 1612–1622. https://doi.org/10.1158/1078-0432.CCR-20-1831.
16. Lièvre, A., Bachet, J.B., Le Corre, D., Boige, V., Landi, B., Emile, J.F., Côté, J.F., Tomasic, G., Penna, C., Ducreux, M., et al. (2006). KRAS mutation status is predictive of response to cetuximab therapy in colorectal cancer. Cancer Res. *66*, 3992–3995. https://doi.org/10.1158/0008-5472.CAN-06-0191.
17. Peeters, M., Douillard, J.Y., Van Cutsem, E., Siena, S., Zhang, K., Williams, R., and Wiezorek, J. (2013). Mutant KRAS codon 12 and 13 alleles in patients with metastatic colorectal cancer: assessment as prognostic and predictive biomarkers of response to panitumumab. J. Clin. Oncol. *31*, 759–765. https://doi.org/10.1200/JCO.2012.45.1492.
18. Moore, M.J., Goldstein, D., Hamm, J., Figer, A., Hecht, J.R., Gallinger, S., Au, H.J., Murawa, P., Walde, D., Wolff, R.A., et al. (2007). Erlotinib plus gemcitabine compared with gemcitabine alone in patients with advanced pancreatic cancer: a

phase III trial of the National Cancer Institute of Canada Clinical Trials Group. J. Clin. Oncol. *25*, 1960–1966. https://doi.org/10.1200/JCO.2006.07.9525.

19. Sklar, M.D. (1988). The ras oncogenes increase the intrinsic resistance of NIH 3T3 cells to ionizing radiation. Science *239*, 645–647. https://doi.org/10.1126/science.3277276.

20. Duldulao, M.P., Lee, W., Nelson, R.A., Li, W., Chen, Z., Kim, J., and Garcia-Aguilar, J. (2013). Mutations in specific codons of the KRAS oncogene are associated with variable resistance to neoadjuvant chemoradiation therapy in patients with rectal adenocarcinoma. Ann. Surg Oncol. *20*, 2166–2171. https://doi.org/10.1245/s10434-013-2910-0.

21. Mak, R.H., Hermann, G., Lewis, J.H., Aerts, H.J.W.L., Baldini, E.H., Chen, A.B., Colson, Y.L., Hacker, F.H., Kozono, D., Wee, J.O., et al. (2015). Outcomes by tumor histology and KRAS mutation status after lung stereotactic body radiation therapy for early-stage non-small-cell lung cancer. Clin. Lung Cancer *16*, 24–32. https://doi.org/10.1016/j.cllc.2014.09.005.

22. Wang, M., Han, J., Marcar, L., Black, J., Liu, Q., Li, X., Nagulapalli, K., Sequist, L.V., Mak, R.H., Benes, C.H., et al. (2017). Radiation Resistance in KRAS-Mutated Lung Cancer Is Enabled by Stem-like Properties Mediated by an Osteopontin-EGFR Pathway. Cancer Res. *77*, 2018–2028. https://doi.org/10.1158/0008-5472.CAN-16-0808.

23. Yang, L., Shen, C., Estrada-Bernal, A., Robb, R., Chatterjee, M., Sebastian, N., Webb, A., Mo, X., Chen, W., Krishnan, S., and Williams, T.M. (2021). Oncogenic KRAS drives radioresistance through upregulation of NRF2-53BP1-mediated non-homologous end-joining repair. Nucleic Acids Res. *49*, 11067–11082. https://doi.org/10.1093/nar/gkab871.

24. Ostrem, J.M., Peters, U., Sos, M.L., Wells, J.A., and Shokat, K.M. (2013). K-Ras(G12C) inhibitors allosterically control GTP affinity and effector interactions. Nature *503*, 548–551. https://doi.org/10.1038/nature12796.

25. Janes, M.R., Zhang, J., Li, L.S., Hansen, R., Peters, U., Guo, X., Chen, Y., Babbar, A., Firdaus, S.J., Darjania, L., et al. (2018). Targeting KRAS Mutant Cancers with a Covalent G12C-Specific Inhibitor. Cell *172*, 578–589.e17. https://doi.org/10.1016/j.cell.2018.01.006.

26. Canon, J., Rex, K., Saiki, A.Y., Mohr, C., Cooke, K., Bagal, D., Gaida, K., Holt, T., Knutson, C.G., Koppada, N., et al. (2019). The clinical KRAS(G12C) inhibitor AMG 510 drives anti-tumour immunity. Nature *575*, 217–223. https://doi.org/10.1038/s41586-019-1694-1.

27. Moore, A.R., Rosenberg, S.C., McCormick, F., and Malek, S. (2020). RAS-targeted therapies: is the undruggable drugged? Nat. Rev. Drug Discov. *19*, 533–552. https://doi.org/10.1038/s41573-020-0068-6.

28. Guo, P. (2010). The emerging field of RNA nanotechnology. Nat. Nanotechnol. *5*, 833–842. https://doi.org/10.1038/nnano.2010.231.

29. Jasinski, D., Haque, F., Binzel, D.W., and Guo, P. (2017). Advancement of the Emerging Field of RNA Nanotechnology. ACS Nano *11*, 1142–1164. https://doi.org/10.1021/acsnano.6b05737.

30. Ghimire, C., Wang, H., Li, H., Vieweger, M., Xu, C., and Guo, P. (2020). RNA Nanoparticles as Rubber for Compelling Vessel Extravasation to Enhance Tumor Targeting and for Fast Renal Excretion to Reduce Toxicity. ACS Nano *14*, 13180–13191. https://doi.org/10.1021/acsnano.0c04863.

31. Li, X., Bhullar, A.S., Binzel, D.W., and Guo, P. (2022). The dynamic, motile and deformative properties of RNA nanoparticles facilitate the third milestone of drug development. Adv. Drug Deliv. Rev. *186*, 114316. https://doi.org/10.1016/j.addr.2022.114316.

32. Shu, Y., Pi, F., Sharma, A., Rajabi, M., Haque, F., Shu, D., Leggas, M., Evers, B.M., and Guo, P. (2014). Stable RNA nanoparticles as potential new generation drugs for cancer therapy. Adv. Drug Deliv. Rev. *66*, 74–89. https://doi.org/10.1016/j.addr.2013.11.006.

33. Gupta, R., Dastane, A.M., Forozan, F., Riley-Portuguez, A., Chung, F., Lopategui, J., and Marchevsky, A.M. (2009). Evaluation of EGFR abnormalities in patients with pulmonary adenocarcinoma: the need to test neoplasms with more than one method. Mod. Pathol. *22*, 128–133. https://doi.org/10.1038/modpathol.2008.182.

34. Shu, D., Li, H., Shu, Y., Xiong, G., Carson, W.E., 3rd, Haque, F., Xu, R., and Guo, P. (2015). Systemic Delivery of Anti-miRNA for Suppression of Triple Negative Breast Cancer Utilizing RNA Nanotechnology. ACS Nano *9*, 9731–9740. https://doi.org/10.1021/acsnano.5b02471.

35. Fleming, J.B., Shen, G.L., Holloway, S.E., Davis, M., and Brekken, R.A. (2005). Molecular consequences of silencing mutant K-ras in pancreatic cancer cells: justification for K-ras-directed therapy. Mol. Cancer Res. *3*, 413–423. https://doi.org/10.1158/1541-7786.MCR-04-0206.

36. Pecot, C.V., Wu, S.Y., Bellister, S., Filant, J., Rupaimoole, R., Hisamatsu, T., Bhattacharya, R., Maharaj, A., Azam, S., Rodriguez-Aguayo, C., et al. (2014). Therapeutic silencing of KRAS using systemically delivered siRNAs. Mol. Cancer Therapeut. *13*, 2876–2885. https://doi.org/10.1158/1535-7163.MCT-14-0074.

37. Yuan, T.L., Fellmann, C., Lee, C.S., Ritchie, C.D., Thapar, V., Lee, L.C., Hsu, D.J., Grace, D., Carver, J.O., Zuber, J., et al. (2014). Development of siRNA payloads to target KRAS-mutant cancer. Cancer Discov. *4*, 1182–1197. https://doi.org/10.1158/2159-8290.CD-13-0900.

38. Xue, W., Dahlman, J.E., Tammela, T., Khan, O.F., Sood, S., Dave, A., Cai, W., Chirino, L.M., Yang, G.R., Bronson, R., et al. (2014). Small RNA combination therapy for lung cancer. Proc. Natl. Acad. Sci. USA *111*, E3553–E3561. https://doi.org/10.1073/pnas.1412686111.

39. Zorde Khvalevsky, E., Gabai, R., Rachmut, I.H., Horwitz, E., Brunschwig, Z., Orbach, A., Shemi, A., Golan, T., Domb, A.J., Yavin, E., et al. (2013). Mutant KRAS is a druggable target for pancreatic cancer. Proc. Natl. Acad. Sci. USA *110*, 20723–20728. https://doi.org/10.1073/pnas.1314307110.

40. Ross, S.J., Revenko, A.S., Hanson, L.L., Ellston, R., Staniszewska, A., Whalley, N., Pandey, S.K., Revill, M., Rooney, C., Buckett, L.K., et al. (2017). Targeting KRAS-dependent tumors with AZD4785, a high-affinity therapeutic antisense oligonucleotide inhibitor of KRAS. Sci. Transl. Med. *9*, eaal5253. https://doi.org/10.1126/scitranslmed.aal5253.

41. Afonin, K.A., Bindewald, E., Yaghoubian, A.J., Voss, N., Jacovetty, E., Shapiro, B.A., and Jaeger, L. (2010). In vitro assembly of cubic RNA-based scaffolds designed in silico. Nat. Nanotechnol. *5*, 676–682. https://doi.org/10.1038/nnano.2010.160.

42. Lee, J.B., Hong, J., Bonner, D.K., Poon, Z., and Hammond, P.T. (2012). Self-assembled RNA interference microsponges for efficient siRNA delivery. Nat. Mater. *11*, 316–322. https://doi.org/10.1038/nmat3253.

43. Li, Z., Yang, L., Wang, H., Binzel, D.W., Williams, T.M., and Guo, P. (2021). Non-Small-Cell Lung Cancer Regression by siRNA Delivered Through Exosomes That Display EGFR RNA Aptamer. Nucleic Acid Therapeut. *31*, 364–374. https://doi.org/10.1089/nat.2021.0002.

44. Awad, M.M., Liu, S., Rybkin, I.I., Arbour, K.C., Dilly, J., Zhu, V.W., Johnson, M.L., Heist, R.S., Patil, T., Riely, G.J., et al. (2021). Acquired Resistance to KRAS(G12C) Inhibition in Cancer. N. Engl. J. Med. *384*, 2382–2393. https://doi.org/10.1056/NEJMoa2105281.

45. Inamura, K., Ninomiya, H., Ishikawa, Y., and Matsubara, O. (2010). Is the epidermal growth factor receptor status in lung cancers reflected in clinicopathologic features? Arch. Pathol. Lab Med. *134*, 66–72. https://doi.org/10.1043/2008-0586-RAR1.1.

46. Agustoni, F., Suda, K., Yu, H., Ren, S., Rivard, C.J., Ellison, K., Caldwell, C., Jr., Rozeboom, L., Brovsky, K., and Hirsch, F.R. (2019). EGFR-directed monoclonal antibodies in combination with chemotherapy for treatment of non-small-cell lung cancer: an updated review of clinical trials and new perspectives in biomarkers analysis. Cancer Treat Rev. *72*, 15–27. https://doi.org/10.1016/j.ctrv.2018.08.002.

47. DeNicola, G.M., Karreth, F.A., Humpton, T.J., Gopinathan, A., Wei, C., Frese, K., Mangal, D., Yu, K.H., Yeo, C.J., Calhoun, E.S., et al. (2011). Oncogene-induced Nrf2 transcription promotes ROS detoxification and tumorigenesis. Nature *475*, 106–109. https://doi.org/10.1038/nature10189.

48. Pietrantonio, F., Vernieri, C., Siravegna, G., Mennitto, A., Berenato, R., Perrone, F., Gloghini, A., Tamborini, E., Lonardi, S., Morano, F., et al. (2017). Heterogeneity of Acquired Resistance to Anti-EGFR Monoclonal Antibodies in Patients with Metastatic Colorectal Cancer. Clin. Cancer Res. *23*, 2414–2422. https://doi.org/10.1158/1078-0432.CCR-16-1863.

49. Gazdar, A.F. (2009). Activating and resistance mutations of EGFR in non-small-cell lung cancer: role in clinical response to EGFR tyrosine kinase inhibitors. Oncogene *28* (*Suppl 1*), S24–S31. https://doi.org/10.1038/onc.2009.198.

50. Shu, D., Shu, Y., Haque, F., Abdelmawla, S., and Guo, P. (2011). Thermodynamically stable RNA three-way junction for constructing multifunctional nanoparticles for delivery of therapeutics. Nat. Nanotechnol. *6*, 658–667. https://doi.org/10.1038/nnano.2011.105.

51. Shu, Y., Haque, F., Shu, D., Li, W., Zhu, Z., Kotb, M., Lyubchenko, Y., and Guo, P. (2013). Fabrication of 14 different RNA nanoparticles for specific tumor targeting without accumulation in normal organs. RNA *19*, 767–777. https://doi.org/10.1261/rna.037002.112.

52. Shu, Y., Shu, D., Haque, F., and Guo, P. (2013). Fabrication of pRNA nanoparticles to deliver therapeutic RNAs and bioactive compounds into tumor cells. Nat. Protoc. *8*, 1635–1659. https://doi.org/10.1038/nprot.2013.097.

53. Sunaga, N., Shames, D.S., Girard, L., Peyton, M., Larsen, J.E., Imai, H., Soh, J., Sato, M., Yanagitani, N., Kaira, K., et al. (2011). Knockdown of oncogenic KRAS in non-small cell lung cancers suppresses tumor growth and sensitizes tumor cells to targeted therapy. Mol. Cancer Therapeut. *10*, 336–346. https://doi.org/10.1158/1535-7163.MCT-10-0750.

54. Yang, L., Shen, C., Pettit, C.J., Li, T., Hu, A.J., Miller, E.D., Zhang, J., Lin, S.H., and Williams, T.M. (2020). Wee1 Kinase Inhibitor AZD1775 Effectively Sensitizes Esophageal Cancer to Radiotherapy. Clin. Cancer Res. *26*, 3740–3750. https://doi.org/10.1158/1078-0432.CCR-19-3373.

OMTN, Volume *33*

Supplemental information

Targeting oncogenic *KRAS* in non-small cell lung cancer with EGFR aptamer-conjugated multifunctional RNA nanoparticles

Linlin Yang, Zhefeng Li, Daniel W. Binzel, Peixuan Guo, and Terence M. Williams

Table S1: Sequences used for construction of 3WJ pRNA nanoparticles.

ID	sequence
a: KRASG12C siRNA sense strand	5'-uuG ccA uGu GuA uGu GGG Guu GGa Gcu uGu GGc GuA Guu-3'
a': Scramble siRNA sense strand	5'-uuG ccA uGu GuA uGu GGG GGu cGA cGu ccA uuA ucu uuu-3'
b: EGFR aptamer strand	5'-ccc AcA uAc uuu Guu GAu ccG ccu uAG uAA cGu Gcu uuG AuG ucG Auu cGA cAG GAG Gc-3'
b': Scramble aptamer strand	5'-ccc AcA uAc uuu Guu GAu ccu ucG uAc cGG GuA GGu uGG cuu GcA cAu AGA AcG uGu ucA-3'
c: Strand without Alexa647	5'-GGA ucA Auc AuG GcA A-3'
c': strand for Alexa647 conjugation	5'-GGA ucA Auc AuG GcA A (C6-NH)(Alexa 647)-3'
d: KRASG12C siRNA antisense strand	5'-cuA cGc cAc AAG cuc cAA-3'
d': Scramble siRNA antisense strand	5'-AAG AuA AuG GAc Guc GAc c-3'

The lower letters indicated 2'-Fluoro modified nucleotides.

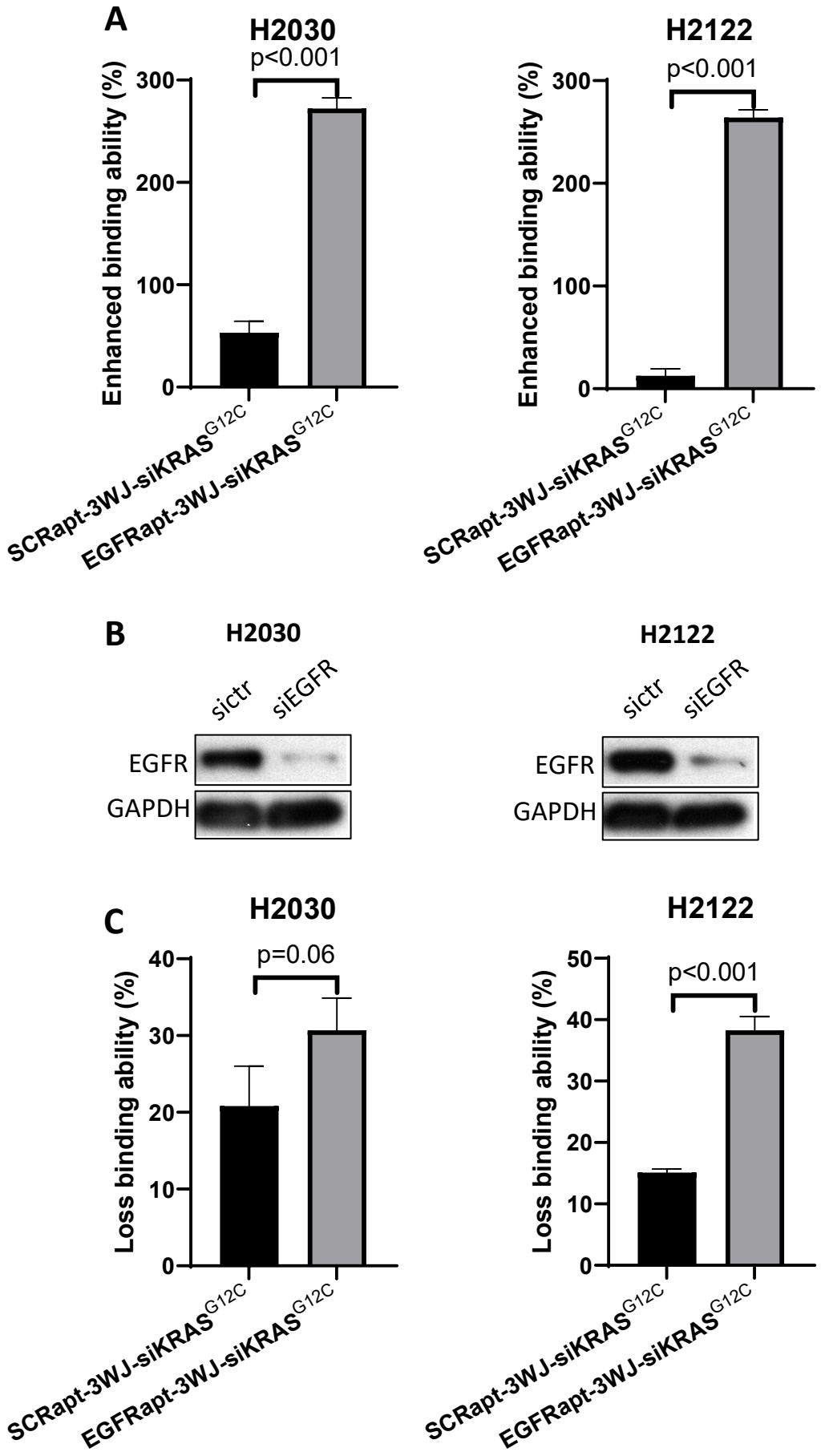

Figure S1. EGFR aptamer increased pRNA nanoparticle binding ability to NSCLC cells. A. Enhanced pRNA binding ability (%) by EGFR aptamer compared to non-aptamer pRNA nanoparticles (SCRapt). **B.** Immunoblotting confirms EGFR silencing by EGFR siRNA. **C.** Reduction in binding ability (%) of pRNA nanoparticles after EGFR silencing in NSCLC cells compared to non-targeting siRNA control cells (sictr).

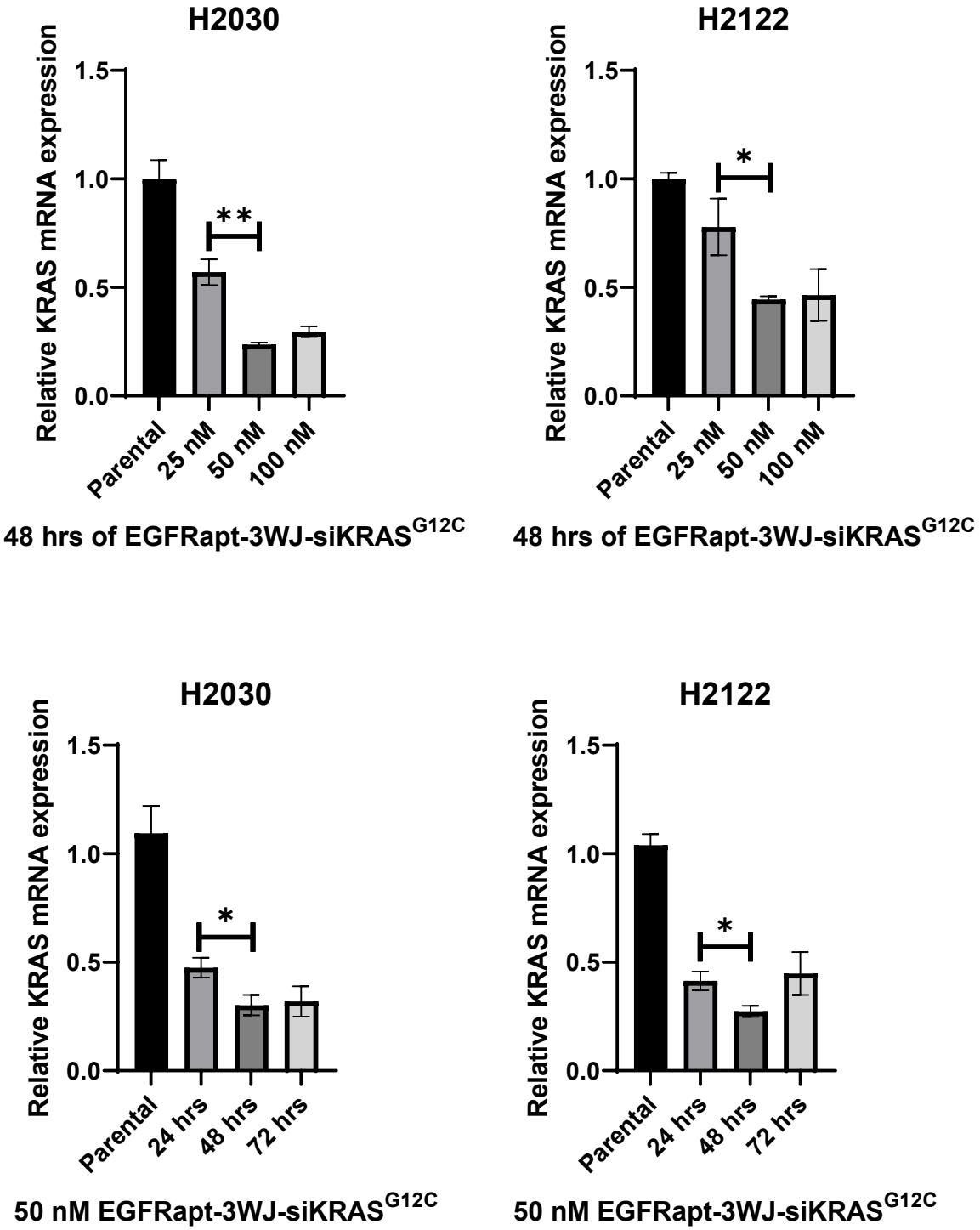

Figure S2. Dose and time course suppression of KRAS mRNA by EGFRapt-3WJ-si*KRAS^{G12C}* nanoparticles

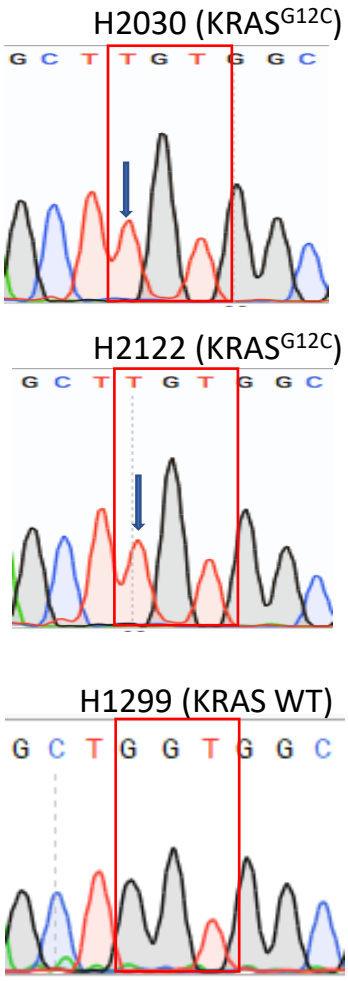

Figure S3. Sanger sequencing confirms the presence of KRAS^{G12C} mutations in H2030 and H2122 cells, and wild-type KRAS in H1299 cells.

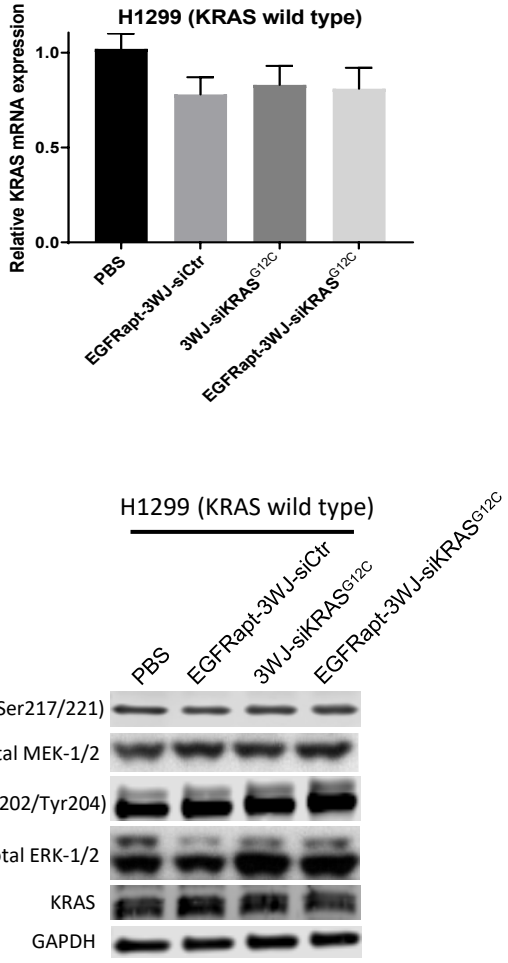

Figure S4. KRAS wild type NSCLC is not a target of $EGFR_{apt}$-3WJ-si*KRAS*^{G12C} pRNA nanoparticles

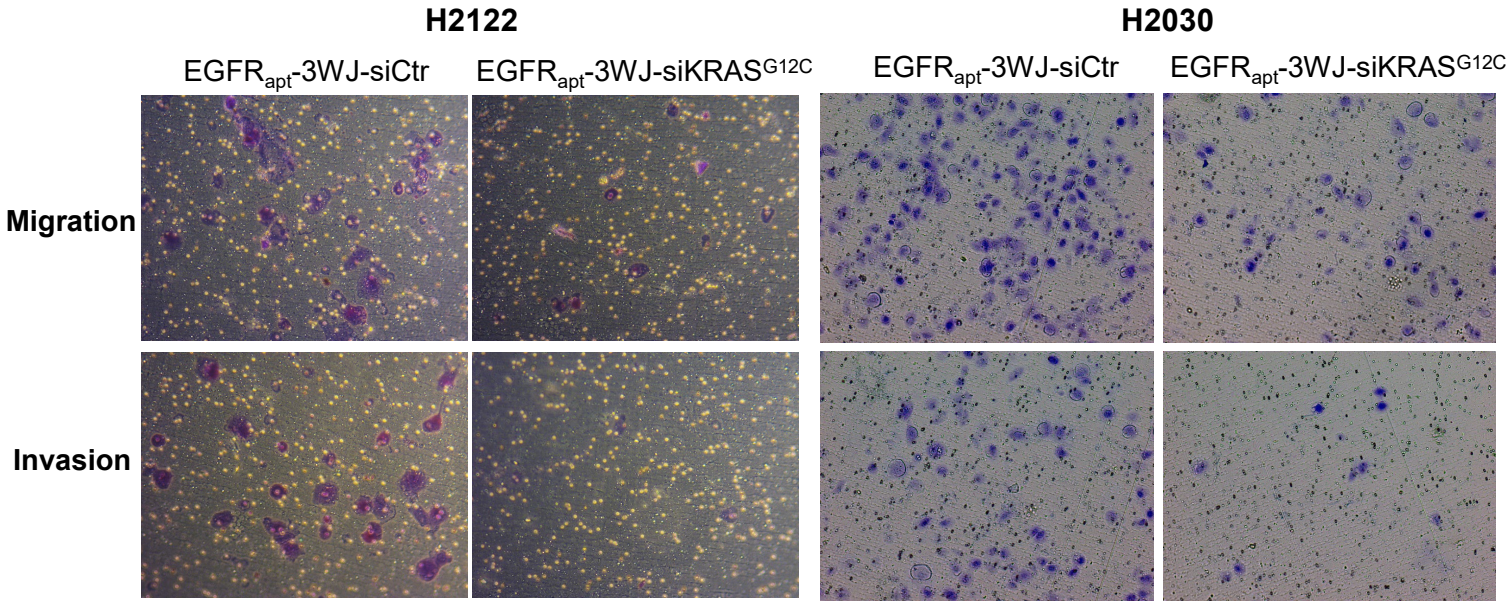

Figure S5. Representative pictures of migration and invasion assays in H2030 and H2122 cells.

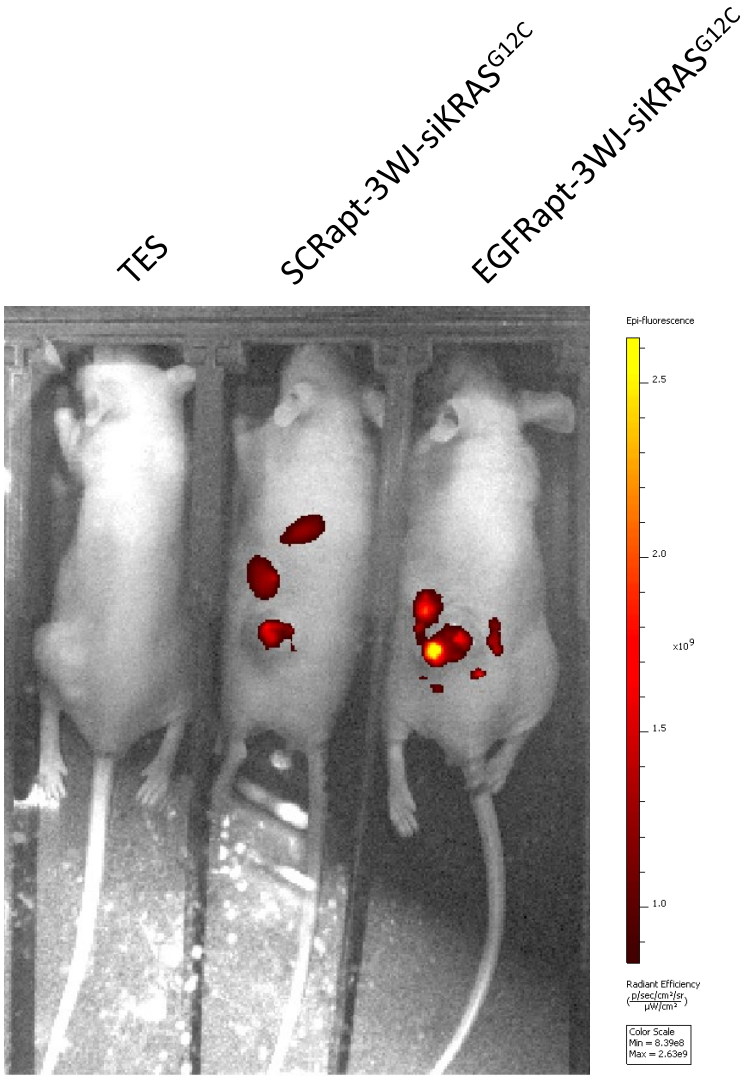

Figure S6. *In vivo* biodistribution of EGFRapt-3WJ-si*KRAS*^{G12C} and SCRapt-3WJ-si*KRAS*^{G12C} in H2122 tumor xenografts.